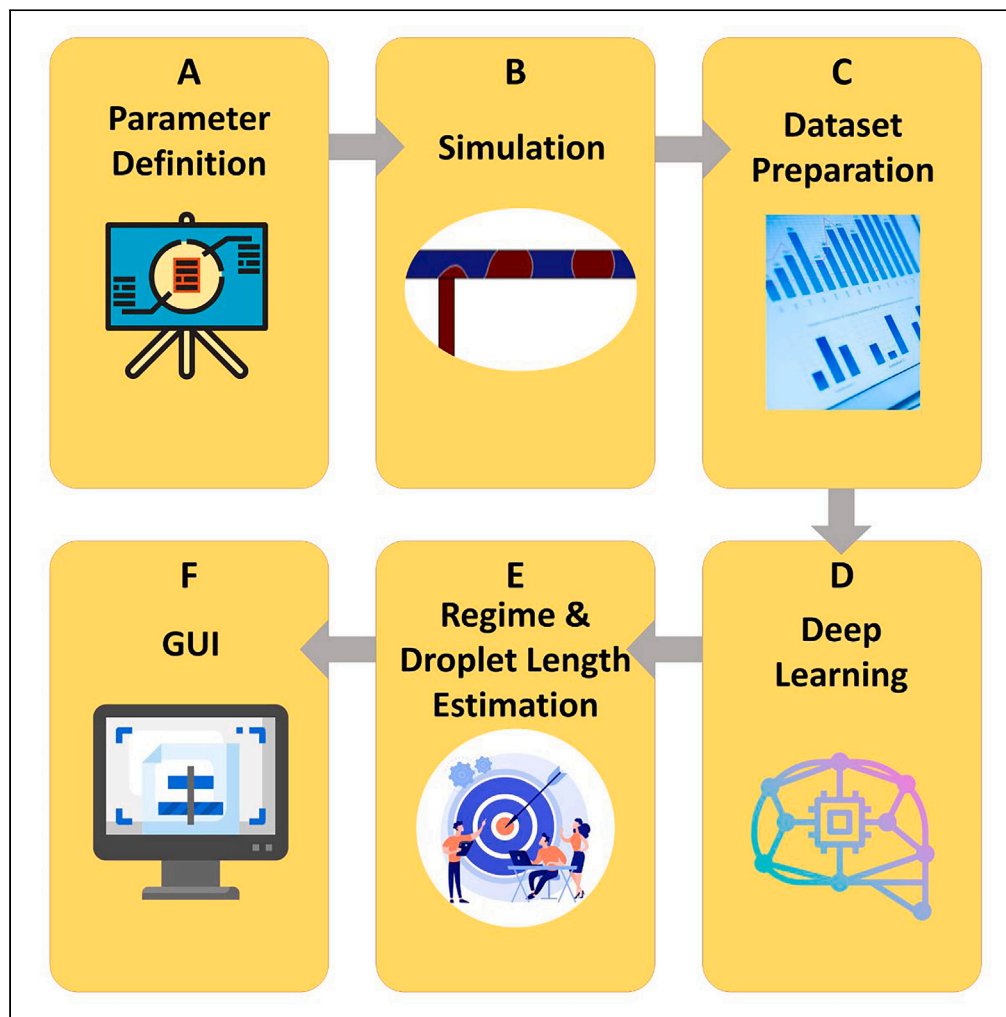


Article

Deep learning-augmented T-junction droplet generation



Abdollah
Ahmadpour,
Mostafa Shojaeian,
Savas Tasoglu

stasoglu@ku.edu.tr

Highlights

Estimation of droplet length and regime in T-junction droplet generator

Utilizing deep learning and machine learning for design parameter estimation

Resulting 2D maps of design parameters for droplet length and regime estimation

Developing GUI for T-junction droplet generator based on tuning input parameters

Ahmadpour et al., iScience 27,
109326
April 19, 2024 © 2024 The
Author(s).
[https://doi.org/10.1016/
j.isci.2024.109326](https://doi.org/10.1016/j.isci.2024.109326)

Article

Deep learning-augmented T-junction droplet generation

Abdollah Ahmadpour,¹ Mostafa Shojaeian,¹ and Savas Tasoglu^{1,2,3,4,5,6,*}

SUMMARY

Droplet generation technology has become increasingly important in a wide range of applications, including biotechnology and chemical synthesis. T-junction channels are commonly used for droplet generation due to their integration capability of a larger number of droplet generators in a compact space. In this study, a finite element analysis (FEA) approach is employed to simulate droplet production and its dynamic regimes in a T-junction configuration and collect data for post-processing analysis. Next, image analysis was performed to calculate the droplet length and determine the droplet generation regime. Furthermore, machine learning (ML) and deep learning (DL) algorithms were applied to estimate outputs through examination of input parameters within the simulation range. At the end, a graphical user interface (GUI) was developed for estimation of the droplet characteristics based on inputs, enabling the users to preselect their designs with comparable microfluidic configurations within the studied range.

INTRODUCTION

Microfluidics has emerged as a promising tool for the manipulation and analysis of small volumes of fluids with microscale dimensions.^{1–6} Microfluidic droplet generation through bringing two or more liquid phases into contact inside microchannels has established a significant research platform for numerous applications such as segmented fluids,⁷ biological assays,⁸ microchemical reactions,^{9–11} drug delivery,¹² single cell analysis,¹³ food engineering,¹⁴ extraction processes,^{15,16} on-chip microfluidic applications,¹⁷ oil recovery,¹⁸ and fuel cell technology.¹⁹ Although more complex geometries have been studied in recent years,^{20,21} simple geometry configurations like T-junctions and flow-focusing droplet generator schemes are still fundamental,²² and are being commonly used to investigate droplet dynamic behaviors^{23–25} and droplet generation²⁶ presenting applications in various fields in many cases.²²

In droplet generators, shear and squeezing forces resulting from meeting continuous and dispersed phase streams lead to droplet formation, where the size and production rate of droplets can be adjusted by their flow rates and the fluid properties of the liquids.²⁷ The production of water droplets in oil in a T-junction microchannel was earlier described by Thorsen et al.,²⁸ and experimental research on some factors influencing droplet formation (e.g., droplet size) in an oil-water system was initially conducted by Nisisako et al.²⁹ Since then, droplet production has been the subject of a huge number of research works.²² In that regard, many experimental investigations have been conducted to study droplet generation in T-junction and flow-focusing microchannels. The flow-focusing microchannel has been a prominent point of experimental investigation, with researchers exploring the effect of various parameters on droplet size control and monodispersity.^{30–32} At the same time, the T-junction microchannel, characterized by its simplicity and ease of integrating several components into a compact space, has been extensively explored in experimental studies. Researchers have investigated the influence of channel geometry, flow rates, and fluid properties on droplet size and its formation.^{33–35} Studies have explored the effects of capillary number, Reynolds number, and surfactant concentration in flow-focusing and T-junction microchannels, revealing some details of the droplet generation process.^{26,36–38} These studies have contributed valuable insights into the fundamental dynamics of droplet formation in flow-focusing and T-junction.

On the other hand, computer-based simulations offer a powerful tool for researchers and engineers to explore the complexities of droplet formation, aiding in the optimization of microchannel designs and operational parameters for various applications. Advanced numerical methods, including finite element methods, lattice Boltzmann simulations, and finite volume methods have been employed to model the dynamic interplay of fluids in microchannels, offering a better understanding of droplet generation processes.^{38–42} Besides, two-phase flow numerical simulations have the potential to provide better insight into the interactions between dispersed and continuous phases, contributing to the prediction and optimization of droplet size distributions.^{24,43}

¹Mechanical Engineering Department, School of Engineering, Koç University, Istanbul 34450, Türkiye

²Koç University Arçelik Research Center for Creative Industries (KUARI), Koç University, Istanbul 34450, Türkiye

³Koç University Is Bank Artificial Intelligence Lab (KUIS AILab), Koç University, Sarıyer, Istanbul 34450, Türkiye

⁴Koç University Translational Medicine Research Center (KUTTAM), Koç University, Istanbul 34450, Türkiye

⁵Boğaziçi Institute of Biomedical Engineering, Boğaziçi University, Istanbul 34684, Türkiye

⁶Lead contact

*Correspondence: stasoglu@ku.edu.tr

<https://doi.org/10.1016/j.isci.2024.109326>



As researchers explore droplet generation through simulations, the synergy between computational tools and experimental validation becomes increasingly apparent. Conducting simulations prior to experimental work significantly improves the comprehension of microfluidic processes, presenting a cost-effective approach for optimizing designs. This is especially pertinent in the context of biomedical applications, where experimental studies can be financially demanding. The significance of fluids, like oil, serving as carriers for cells in droplet-based microfluidic devices designed for single-cell or microtissue analysis underscores the importance of gaining a general understanding of how the properties of these fluids impact the overall process of droplet formation.^{44,45} Simulations allow for a thorough exploration of the system dynamics, aiding researchers in refining microfluidic designs and minimizing the need for resource-intensive experimental iterations.⁴⁶ In particular, integrating droplet microfluidics with machine learning (ML), deep learning (DL), and artificial intelligence (AI) tools can be a tremendous practical strategy to build up an automated droplet-based microfluidics platform for processing huge quantities of data.^{5,47–51} It has been effectively demonstrated that AI tools can automate the most complicated systems.^{48,52–54} Automation of the complete microfluidic system, from flow control to droplet classification, is conceivable with proper training and the use of optimal ML models.^{55–57} In a study, a web-based tool was introduced that harnessed ML techniques to anticipate the droplet diameter and flow rate for flow-focusing droplet generators.⁴⁷ While the flow-focusing droplet generation properties have been estimated and simulated via ML tools,^{47,58,59} the prediction of droplet formation using a combination of simulation and AI estimation for a T-junction microchannel has still remained unexplored in the literature. In this study, we established a parametric design for T-junction microfluidic droplet generators, utilizing finite element method (FEM) simulations via COMSOL Multiphysics software. This allowed for a comprehensive investigation of various fluid properties, fluidic conditions, and fluid-wall interaction on both the resulting droplet length and the associated production regime. To validate the FEM, we conducted a comparison between the simulation results and relevant experimental data available in the literature, apart from a mesh dependency study. Subsequently, a dataset was collected to train ML and DL algorithms, enabling the prediction of desired outputs. Finally, a graphical user interface (GUI) was developed to estimate the outputs based on arbitrary and optimal estimation models.

RESULTS

Simulation

In this study, we have numerically investigated two-phase flows inside T-junction microchannels using COMSOL Multiphysics software. The mathematical model was constructed based on a 2D, laminar, two-phase flow with the available modules in the software. The governing equations are mathematically described by the mass continuity (Equation 1) and momentum equations (Equation 2), as follows:

$$\nabla \cdot \mathbf{u} = 0 \quad (\text{Equation 1})$$

$$\rho(\varphi)[\partial \mathbf{u} / \partial t + \mathbf{u} \cdot \nabla \mathbf{u}] = -\nabla p + \nabla \cdot \boldsymbol{\tau} + \mathbf{F}_\sigma \quad (\text{Equation 2})$$

where \mathbf{u} and p are the velocity vector and pressure fields, respectively. To account for implementing two-phase model, the level set function (φ) was employed as a continuous step function. Within one fluid domain, φ has a value of 0, while in the other fluid domain it is 1. The range of the variable φ was therefore limited to the interval $0 \leq \varphi \leq 1$. Moreover, the interface between the two fluids in the two-phase flow was defined by the value $\varphi = 0.5$. The relationship between the deviatoric stress tensor ($\boldsymbol{\tau}$) and the rate of deformation tensor (\mathbf{D}) is as

$$\boldsymbol{\tau} = 2\mu(\varphi)\mathbf{D} \quad (\text{Equation 3})$$

where

$$\mathbf{D} = 0.5 \left[(\nabla \mathbf{u}) + (\nabla \mathbf{u})^T \right] \quad (\text{Equation 4})$$

The density (ρ) and dynamic viscosity (μ) of the two-phase system are as

$$\rho(\varphi) = \rho_c + (\rho_d - \rho_c)\varphi \quad (\text{Equation 5})$$

$$\mu(\varphi) = \mu_c + (\mu_d - \mu_c)\varphi \quad (\text{Equation 6})$$

where the subscripts 'c' and 'd' denote the continuous and dispersed phases, respectively.

The interfacial force (\mathbf{F}_σ) between the two fluids is also determined by

$$\mathbf{F}_\sigma = \sigma \kappa \delta(\varphi) \mathbf{n} \quad (\text{Equation 7})$$

where σ represents the interfacial tension (in mN/m), κ refers to the curvature of the interface, $\delta(\varphi)$ represents the Dirac Delta function, and \mathbf{n} denotes the unit normal vector.

The microfluidic configuration for droplet generation simulations was a T-junction microchannel, as previously mentioned, with dimensions in accordance with the previous experimental study,⁶⁰ as depicted in Figure 1A. The demonstration of the geometry (Figure 1B) consisted of two perpendicular microchannels with a width of 65 μm for the continuous phase (CP) microchannel and 51 μm for the dispersed phase (DP) microchannel that made a junction at a distance of 200 μm from the CP microchannel. To validate our simulations, we compared the simulation results with the experimental results of.⁶⁰ A shallow channel approximation was used to enhance the 2D simulation results according to the previous experimental depth of the microfluidic chip,⁶⁰ which was 30 μm . The sunflower oil was considered as CP entering the

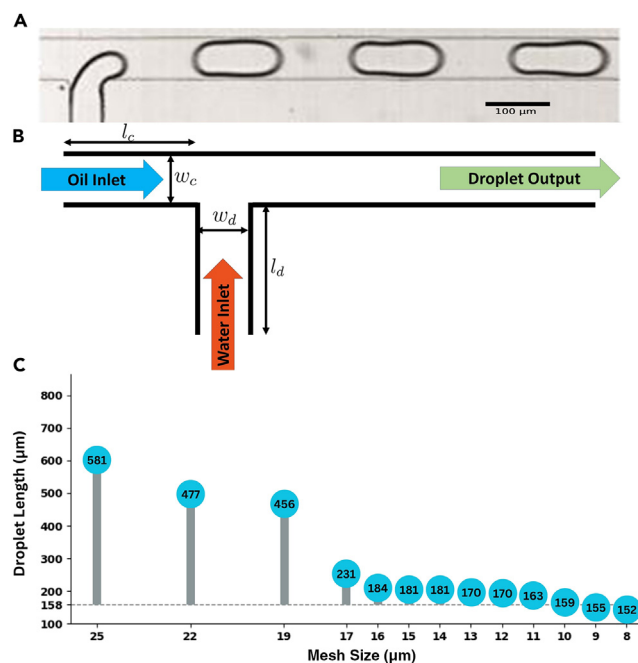


Figure 1. Microchannel design for T-junction droplet generation and mesh convergence analysis

(A) Previous experimental study⁶⁰ on creating water droplets in sunflower oil medium (scale bar, 100 μm). The oil and water microchannels in the microfluidic device were both flowing at a rate of 50 ml/h. The viscosity of oil and water were 53.5 mPa.s and 1 mPa.s, respectively. The contact angle between the oil and the microchannels was $\pi/8$ rad, and that of water was $3\pi/5$ rad. The interfacial tension between the oil and water was 23.5 mN/m.

(B) Dimensions of T-junction microchannels used in the experimental study⁶⁰: $l_c = l_d = 200$ μm , $w_c = 65$ μm and $w_d = 51$ μm .

(C) Convergence plot illustrating the relationship between mesh refinement and the resulting droplet length in the T-junction microchannel model. The droplet length of 159 μm with the maximum mesh size of $\Delta_{\text{max}}(\mu\text{m}) = 10$ μm was the closest calculated droplet length to the measured droplet length in the experimental study by⁶⁰ which was 158 μm . See also Figure S1. Subfigure (A) was reproduced from⁶⁰ with permission from AIP Publishing.

main channel, chosen from the material library in COMSOL software. Water as DP was taken in from side channel. The two fluids entered from inlets met at the junction, flowing downstream of the main channel, producing droplets. The outlet of the CP channel was open to the ambience, with the outlet pressure set at zero Pa.

Mesh independent study







The accuracy of numerical results is also dependent on the mesh properties employed for the discretization of the computational domain. A mesh independence study was carried out to obtain an optimal mesh, balancing result accuracy and computational cost. To investigate the effect of mesh size on the droplet length formed at the microchannel junction, a mesh independence analysis was performed, as depicted in Figure 1C. The analysis encompassed maximum mesh element sizes (Δ_{max}) ranging from 25 to 8 μm . Table 1 presents the mesh convergence analysis, illustrating the impact of varying triangular mesh sizes and the total number of mesh elements on the effective droplet formation for the discussed FEM model. The results demonstrated that the stability of droplet behavior, including formation and length, was greatly increased with a decrease in Δ_{max} down to 11 μm , and a mesh element count exceeding 3200. Further refinement of the mesh had a negligible impact on the results for $\Delta_{\text{max}} < 10$ μm , thus indicating that a mesh size of $\Delta_{\text{max}} = 10$ μm was sufficient to obtain mesh-independent simulation results. This mesh size also correlated effectively with the experimental study by,⁶⁰ yielding a simulated droplet length of 159 μm that closely matched the measured droplet length of 158 μm in the mentioned reference. Therefore, the subsequent results presented herein are obtained using a non-uniform triangular type with a mesh size of $\Delta_{\text{max}} = 10$ μm and 3564 mesh elements. Figure S1 compares the simulation results when the optimal mesh size was selected and the experimental study,⁶⁰ and a good agreement between the simulation and experimental results is seen.

DISCUSSION

Estimation process

The main focus of the study is to establish a relationship between input parameters and two critical output variables: droplet length and regime. The first step involved FEM simulations, wherein the interaction between oil and water was simulated, leading to the production of phase-defined droplets. Four main input parameters were defined to describe the system: (I) Flow Rate Ratio (Q_r), (II) Capillary Number (Ca), (III) Wettability of the CP (θ_c) and (IV) Wettability of the DP (θ_d). Through the Livelink MATLAB transcript function, images of the generated

Table 1. Data from mesh independence study

Δ_{max} (μm)	Number of mesh elements	Generated Droplet
13	2060	
12	2619	
11	3213	
10	3564	
9	4485	
8	5591	

Non-uniform two-dimensional triangular mesh was used for the T-junction microchannel geometry. The interface separating the two fluids in the two-phase flow was characterized by a value of $\phi = 0.5$.

droplets were captured and stored (Figure 2A). Subsequently, FEA and image processing were conducted to convert these images into a binary format, enhancing the accuracy of measuring droplet length (Figure 2B). From the processed images, two essential outputs, i.e., the regime and the droplet length, were extracted (Figure 2C). A dataset was created to involve generated images for various input parameters, resulting in a large dataset comprising 8020 data points. Table 2 lists the values for the input parameters that were used for creating the dataset. Each set of inputs resulted in two outputs, the corresponding regime associated to the droplets produced and the droplet length (Figure 2D). With the dataset, ML and DL algorithms were developed to train a model to understand and estimate the dynamic relationship between input parameters and the resulting outputs (Figure 2E). Classification models were utilized to train the droplet generation regime, while regression models were employed to train numerical droplet length outputs. Furthermore, artificial neural networks (ANNs) were designed and trained to investigate and compare the effectiveness of the trained estimation models. The trained models were used to estimate the key outputs for the droplet generation setup (Figure 2F). Moreover, all classification, regression, and ANN methods were executed using Python.

Regime estimation

It was observed that the variation of the four input parameters can lead to formation of four different droplet regimes, which are (1) Dripping, (2) Squeezing, (3) Jetting, and (4) Co-flow (Figure 3A). The droplets produced in the 'Squeezing' regime are more stable than those produced in the other regimes. This superiority could be attributed to the generation of more uniform droplets in size. To determine the regime corresponding to each data point, an image analysis approach was applied to the dataset images produced by simulations. Subsequently, a range of well-established classification and ANN models were employed for the purpose of training. The dataset was partitioned into two segments to establish distinct data points for the training of models and their subsequent evaluations. The training set encompassed 80% of the entire dataset, while the remaining 20% of the dataset served as a test set for the assessment of trained models.

Classification models are a type of ML model that is designed to categorize input data into one or more predefined classes or categories. The classification models employed for training the dataset were logistic regression, k-nearest neighbor (KNN), support vector machine (SVM), Kernel SVM, Naive Bayes, decision tree, and random forest. After applying each trained model to the test set, an R2 score was computed for the evaluation of model performance. The R2 score represents a statistical metric utilized to ascertain the proportion of variance

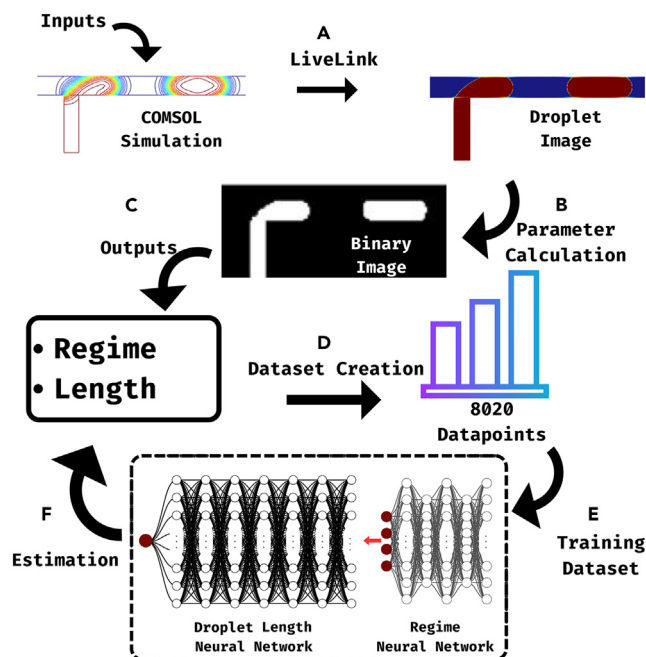


Figure 2. Dynamic process of the study based on the T-junction droplet simulations

(A) The COMSOL simulation resulted in a phase description of the final generated droplets, stemming from the settings initialized for interaction between oil and water, which was then conducted using the LiveLink MATLAB transcript function of the software to create and store images of phase-defined generated droplets for various input parameters.

(B) Images resulting from FEA were then subjected to an image analysis process in which a binary format of those images was used to enhance the performance of measuring parameters visualized in the droplet formation.

(C) According to measured variables in binary images, two important output parameters were extracted that emphasize the goal of the current research: Regime and Droplet Length.

(D) In each scenario of image creation, four main inputs resulted in two numerical outputs, which were then ordered in a table to create a dataset of 8020 data points.

(E) The resulting dataset was then trained with ML and DL methods, including classification models to train the droplet generation regime and regression models with the purpose of training-droplet length.

(F) Finally, the trained models were used to estimate the main outputs for the proposed T-junction droplet generation setup.

in an output that can be predicted or elucidated by input parameters. After conducting a thorough assessment of the performance metric R2 score, the Decision Tree classification model with an R2 score of 0.998, denoted as the ML_R , was chosen for categorizing the dataset to estimate the regimes of droplet generation model (Table S1). Decision trees are versatile ML models, employing a hierarchical structure to make decisions based on input features.^{61,62} In a decision tree, decision nodes (points where the algorithm makes decisions or splits in the data based on specific features) contain conditions that guide the data down different branches of the tree, and final leaf nodes then hold the predicted output. At the end, the chosen model was implemented for the entire dataset to determine the droplet regimes.

Another potential approach to classify the droplet regime is through the application of ANNs. An ANN is a computational model inspired by the structure and functioning of the human brain's neural networks, featuring interconnected nodes organized into layers, including input, hidden, and output layers.⁶³ These nodes are connected by weighted connections, and the corresponding network learns by adjusting these weights during a training process based on input data and desired output. The architecture that was used for regime classification consisted of a total of 6 layers that were fully connected to each other, including 4 hidden layers with several neurons of 6, 18, 6, and 18 in each of them, respectively. The input layer consisted of 18 neurons, while the output layer consisted of 4 neurons, representing the main four outputs for the

Table 2. Determined values of each input parameters

Inputs	Values
Flow Rate Ratio (Q_c)	0.1, 0.2, 0.4, 0.6, 0.8, 1, 2, 4, 6, 8, 10
Capillary Number (Ca)	1e-4, 1e-3, 1e-2, 2e-2, 5e-2, 8e-2, 0.1, 0.5, 1
Wettability of Continuous Phase (θ_c°)	10, 20, 30, 40, 50, 60, 70, 80, 90
Wettability of Continuous Phase (θ_d°)	10, 20, 30, 40, 50, 60, 70, 80, 90

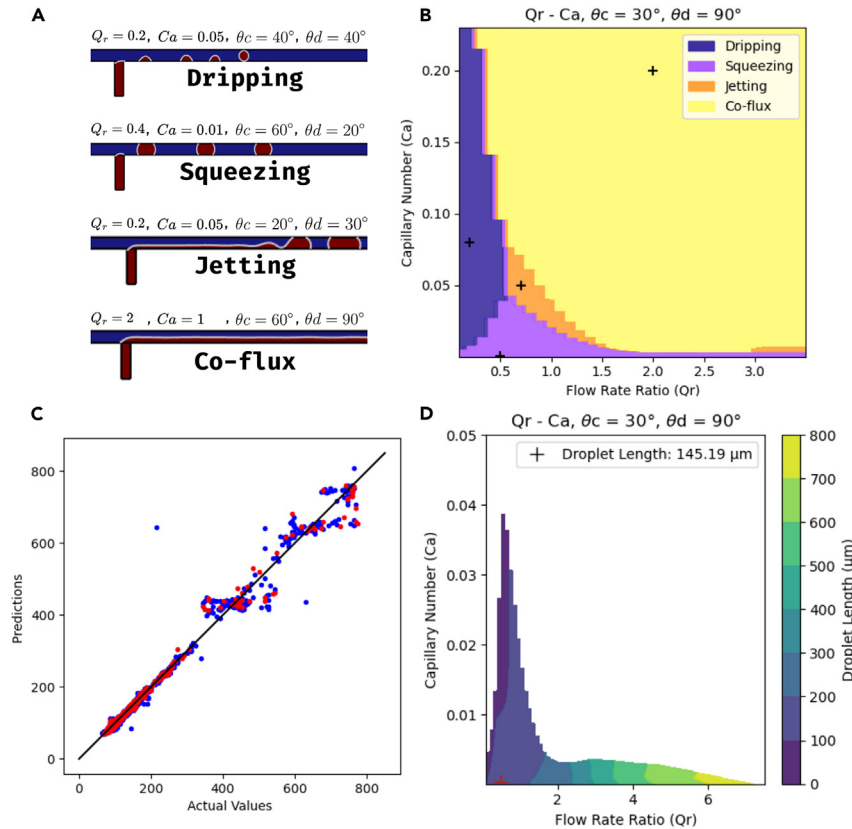


Figure 3. Estimation of the droplet regime and length using trained DL models

(A) Demonstration of four different droplet formations and regimes achieved by their corresponding input parameters.

(B) The result of the DL_R model in a 2D plot, where variations in Q_r and Ca were illustrated while maintaining constant values for θ_c and θ_d to facilitate accurate estimation of the regimes for the specified parameters. The marked datapoints (from²⁶) represent four points within the categorized regimes, with $Q_r = 0.5$ and $Ca = 0.0003$ for 'Dripping', $Q_r = 0.2$ and $Ca = 0.08$ for 'Squeezing', $Q_r = 0.7$ and $Ca = 0.05$ for 'Jetting' and $Q_r = 2$ and $Ca = 0.2$ for 'Co-flux'.

(C) The performance of the DL_L model by comparing the predicted and calculated values in both the training (blue) and test (red) datapoints.

(D) A 2D plot generated by the DL_L model, depicting varying Q_r and Ca while maintaining constant values of 30° and 90° for θ_c and θ_d , respectively. The marked datapoint (from²⁶) represents the point within the 'Squeezing' regime, with $Q_r = 0.2$ and $Ca = 0.08$. See also [Figures S2–S7](#) and [Tables S1–S4](#).

regimes. An exponential linear unit (ELU) activation function was used for the entire learning network, which applies non-linearity to the network to learn complex patterns and relationships in data occurring during training when gradients become extremely small. Then, a Softmax activation function was used to convert vectors of real numbers into a probability distribution for the output layer, allowing the network to model and predict multiple classes in a mutually exclusive scenario. The model was then optimized by minimizing the loss value and maximizing the accuracy of the training process, which was calculated as the ratio of correctly predicted instances to the total number of instances. The loss value was calculated using [Equation 8](#):

$$\text{Loss} = -\frac{1}{N} \sum_{i=1}^N \sum_{j=1}^c y_{ij} \log(p_{ij}) \quad \text{Equation 8}$$

where N is the number of examples in the batch, C is the number of classes, y_{ij} is an indicator that is between 0 and 1 according to the not-being or being in the correct class, and p_{ij} is the predicted probability of each input. [Figure S2](#) shows the loss value convergence of the training and validation processes according to the number of epochs used in each step. Based on the optimized accuracy of the model with a value of 0.986, this architecture was used to group the dataset and estimate the regimes of droplet generation, denoted as the DL_R model.

To evaluate the ML_R and DL_R models for regime identification in this study, twenty pairs of parameters set of Q_r and Ca of different values with contact angles fixed as 30° and 90° for θ_c and θ_d , respectively, were simulated using FEM. It is worth noting that the parameter set was selected to ensure the absence of any data points not found in the original dataset, training set, or test set. These points were distinct from those encountered by the estimator models during their training and evaluation processes ([Figure S3](#)). The simulation results were then compared with the ML_R and DL_R predictor models ([Table S2](#)). The findings indicate that the DL_R model outperformed the ML_R model, correctly estimating 80% of validation points compared to the ML_R model's 70%. To further evaluate the DL_R architecture model for regime

determination, four distinct values for Q_r and Ca , corresponding to the delineated regimes, were adopted from a study by²⁶ and employed as input parameters for the estimation of droplet generation regimes. We have selected the following data points from²⁶ translated to our regime definitions as: $Q_r = 0.2$ and $Ca = 0.08$ for Dripping, $Q_r = 0.5$ and $Ca = 0.0003$ for Squeezing, $Q_r = 0.7$ and $Ca = 0.05$ for Jetting, and $Q_r = 2$ and $Ca = 0.2$ for Co-flux. The corresponding contact angles were also assumed to be at $\theta_c = 30^\circ$ and $\theta_d = 90^\circ$. Figure 3B illustrates the outcomes of the DL_R model through a 2D plot, demonstrating accurate estimation of the regimes with our DL_R model in agreement with the results of.²⁶ The resulted plot for the ML_R model is additionally depicted in Figure S4, showing the accurate performance of the mentioned four points from²⁶ for regime estimation. Based on the overall evaluation of the models used for regime estimation, the DL_R model architecture was selected for the classification of four distinct regimes in this study.

Droplet length estimation

To estimate the droplet length, the regression and ANN models were examined. Regression models are a type of statistical model used in ML to predict a continuous target variable based on one or more input features. Before proceeding with the regression models, the predicted regimes from the previous step were used as an indicator for droplet length calculation. The 'Squeezing' regime is characterized by easily calculable droplet lengths, while the 'Dripping,' 'Jetting,' and 'Co-flux' regimes correspond to cases where either a non-uniform sequence of droplets is produced, or no droplets exist. Therefore, it is not necessary to calculate and estimate the droplet length for the regimes other than the squeezing regime. The ANN classification model, the DL_R model, was employed to categorize the entire dataset into four regimes, and the corresponding 'Squeezing' regime was only considered for the purpose of droplet length estimation.

The next step was the application of regression and ANN models to parameter sets for the 'Squeezing' category. The regression models considered for the training tasks were linear, multiple linear, polynomial, support vector regression (SVR), decision tree, and random forest. For each trained model applied to the test set, an R2 score was computed, assessing the performance of the regression model. After evaluation of the R2 scores, the polynomial regression model, denoted as the ML_L, with an R2 score of 0.984, was chosen for the calculation and estimation of droplet length within the dataset range (Table S3). The predictions obtained by the Polynomial regression model (ML_L) yielded highly pertinent results within the 'Squeezing' regime. Despite further efforts, extending the application of this model to estimate droplet length in other regimes failed, as expected before, due to the lack of a uniform droplet sequence.

Like in the previous section, another method for computing the droplet length can be employing ANNs for regression purposes. The architecture utilized for droplet length regression comprised a total of 8 fully connected layers, including 6 hidden layers with 32 neurons each. The input layer featured 32 neurons, and the output layer had a single neuron representing the primary output for droplet length. A Rectified Linear Unit (ReLU) activation function was applied across the entire network to introduce non-linearity. The model underwent optimization by minimizing a custom Huber loss function during the training process. In Figure S5, the convergence of loss values in the training and validation processes is depicted based on the number of epochs utilized in each step. With an optimized R2 score of 0.985, this architecture was employed, denoted as the DL_L model, for estimation of the droplet length within the 'Squeezing' regime. Figure 3C depicts the performance of the DL_L model through a comparison between the predicted and computed values within the training set and the test set, illustrating the accuracy of the DL_L model.

To validate the ML_L and DL_L models for droplet length estimation, thirty pairs of parameters set of Q_r and Ca with fixed contact angles of $\theta_c = 30^\circ$ and $\theta_d = 90^\circ$ were simulated using FEM (Figure S6). Similar to the regime identification case, the parameter set was chosen to guarantee the exclusion of any data points not present in the original dataset, training set, or test set. These points were different from those encountered by the estimator models during their training and evaluation processes. For better illustration, the simulation results derived from the plot in Figure S6 are tabulated in Table S4 and compared with the ML_L and DL_L models. The results revealed that the DL_L model gave a better fit to the simulation results compared with the ML_L model, demonstrating predominantly errors below 10%. By contrast, the ML_L model exhibits that over 37% of the validation points have errors exceeding 10%. To further evaluate the DL_L model, one set of input parameters selected in the previous section from²⁶ pertaining to the 'Squeezing' regime was utilized to predict droplet length, as marked in Figure 3D. This figure illustrates a 2D plot generated by the DL_L model, illustrating the variation of Q_r and Ca for constant contact angles of $\theta_c = 30^\circ$ and $\theta_d = 90^\circ$. The color bar denotes droplet length, with white areas indicating a regime other than the 'Squeezing' regime. The plot in Figure S7A illustrates the ML_L model performance, showing a good agreement between the actual and predicted values for both the training and test sets. Figure S7B similarly presents results comparable to those in Figure 3D but using the ML_L model. Based on the overall evaluation of the models used for droplet length estimation, the DL_L model was the best model for droplet length prediction for the 'Squeezing' regime in this study.

Two-dimensional maps for input parameters

After the best models were achieved, the estimation of the regime and droplet length could be carried out using each set of the four input parameters, provided they were defined within a valid range as specified in this study. Consequently, the validity of the estimation, with the mentioned accuracy of the models, depended on input parameters that were not beyond the range established by the original dataset preparation input values (Table 2). The final regime and droplet length were estimated by the models considering all four input parameters and their correlations. In this context, correlations were understood as the statistical assessment of the degree and direction of linear relationships between the primary input parameters and the output variable, elucidating the impact of these parameters on the overall outcome. To estimate an output, whether it is droplet length or regime, the four specified input parameters were utilized, rendering the nature of these dimensions as 4D. The inherent complexity of this 4D space poses challenges for visualizing relationships between the different parameters. To gain insights into the interconnections of these input parameters, the concept of 2D maps was employed. In this approach, to visualize the

collaboration of four parameter sets, two parameters are held constant while the rest are varied in a 2D plot. The color in the resulting 2D space indicates the output of the model. Given the four input parameters, a minimum of six 2D maps is required to comprehensively illustrate all relationships between them. For a better understanding of the effects of each input parameter on the final output, correlations of the main input parameters on the output were calculated. According to the correlations of the input parameters on the regime estimation, the parameters that had more effect on the final decision of the droplet regime production were Q_r and Ca , with correlations of 0.481 and 0.323, respectively, against almost zero correlations for θ_c and θ_d (Figure S8). Based on the calculated correlations, the 2D map that contains Q_r and Ca is the best indicator for regime map representation in this study. Figure 4A shows a complete set of six 2D maps for a set of arbitrary input parameters ($Q_r = 0.5$, $Ca = 0.0003$, $\theta_c = 30^\circ$, and $\theta_d = 80^\circ$) in the ‘Squeezing’ regime predicted by the DL_R model, marked in the plots with ‘+’ sign. The resulting 2D maps illustrate the impact of varying one pair of inputs as a variable, while holding the other constant. As seen, despite the DL_R predicting the ‘Squeezing’ regime, two of the 2D maps exhibit mispredictions. The underlying reason is that the overall map of the four parameters constitutes a 4D space map inherently, and as a result, certain 2D plots, such as the ones here, may not accurately represent the complete map but rather only a projected plot. Therefore, a 4D map would be the best representative for such a case, and as discussed before, the Q_r – Ca map can be regarded as the best illustration representing the regime map. The 2D maps resulted from other arbitrary set of parameters corresponding to the other regimes are illustrated in Figures S9–S11, where the same explanations seem to be relevant. The same approach was considered for finding correlations with droplet length for input parameters. Likewise, the results showed that the parameters Q_r and Ca , with the associated correlations of 0.974 and -0.292 , could be the best parameter pairs to illustrate droplet length (Figure S12), supporting the representation of the Q_r – Ca map as the best indicator for the droplet length map among others. For droplet length estimation, Figure 4B shows a complete set of 2D maps for a set of input parameters in the ‘Squeezing’ regime for the values given in Figure 4A. The 2D maps for the droplet length of three other points from the validation points specified in the regression verification section (sec. 3.3) are illustrated in Figures S13–S15, showing the effect of changing each pair of input parameters on the estimated droplet length. The estimated value for droplet length is represented by the color bar. Regions with no droplet length information in the maps indicate areas where the combination of input parameter pairs is inferred to result in a “non-squeezing” regime, characterized by either the absence of droplet generation in the system or the lack of a uniform sequence of droplets, as mentioned in section 3.3. As a consequence, for each set of the four input parameters within the valid range determined by this study, a complete set of twelve 2D maps can be created to depict the estimated regime and droplet length. These maps illustrate the estimated regime and droplet length, along with the variations in outputs that can be estimated by adjusting each pair of input parameters.

Graphical user interface (GUI)

Leveraging the impact of four input parameters on two-phase flow characteristics for droplet generation, a GUI was created using the DL_R and DL_L models for regime and droplet length estimation (Figure 5). This interface facilitates the prediction of new outcomes when adjustments are made to these parameters. The created GUI encompasses two sets of 2D maps of input parameters for both droplet length and regime estimation. The left side of the GUI application illustrates the schematic of the microchannel geometry, and the right side provides instructions for the developed GUI. This includes details regarding the valid parameter range, the geometrical parameters utilized in the study, and the hydraulic diameter of the designed CP microchannel. Video S1 demonstrates the functionality of the developed GUI as operated by a user. When the “Calculate” button is clicked, the GUI will generate six sets of 2D maps pertaining to the estimation of droplet length. Additionally, it will provide the estimated regime and droplet length for the input values entered. The user can choose to switch between sets of 2D maps related to regime by clicking “Regime 2D maps” or return to droplet length-related 2D maps by clicking “Length 2D maps.” Users can also observe the impact of input parameters on the eventual regime or droplet length by adjusting the input parameters based on the generated 2D maps at each stage, enabling them to attain the desired output regime and droplet length.

In conclusion, droplet generation in the T-junction microchannel was simulated using COMSOL Multiphysics software, a finite element analysis-based tool, whose results were encoded with input parameters. The LiveLink functionality was utilized for image analysis to identify the droplet regimes and calculate droplet length for a particular regime. ML and DL algorithms were applied to the collected datasets extracted from the simulations to enable prediction of droplet regime and droplet length. A validation was also made by comparison of the simulation against the experimental data for a case, from the literature, and a mesh independence test was examined as well. The estimation process involved the creation of a dataset through simulations and image calculations. Excellent performance in regime estimation was demonstrated by the chosen ANN classification model (DL_R model), achieving an accuracy of 0.986. The DL_L model as an ANN model for regression purposes, with an R^2 score of 0.985, was successful in estimating the droplet length for existing droplets. Comprehensive investigations were made to include the generation of 2D maps illustrating the relationships between input parameters in determining outputs. All attempts resulted in the development of a GUI to facilitate rapid estimation of simulation results based on the input parameters designed for the T-junction droplet generator. The ongoing study advances comprehension and accelerates insights into the droplet generation process, providing valuable AI estimation tools for designing and optimizing droplet-based microfluidic devices, which can be fine-tuned for specific applications in industries, clinics, and experimental laboratories.

Limitations of the study

This study is particularly relevant for advanced experiments like single-cell analysis, where fluid properties significantly influence droplet formation within the system. Further investigation into viscosity, interfacial tension, and wettability is necessary for specific applications involving fluids other than oil and water studied in this context.

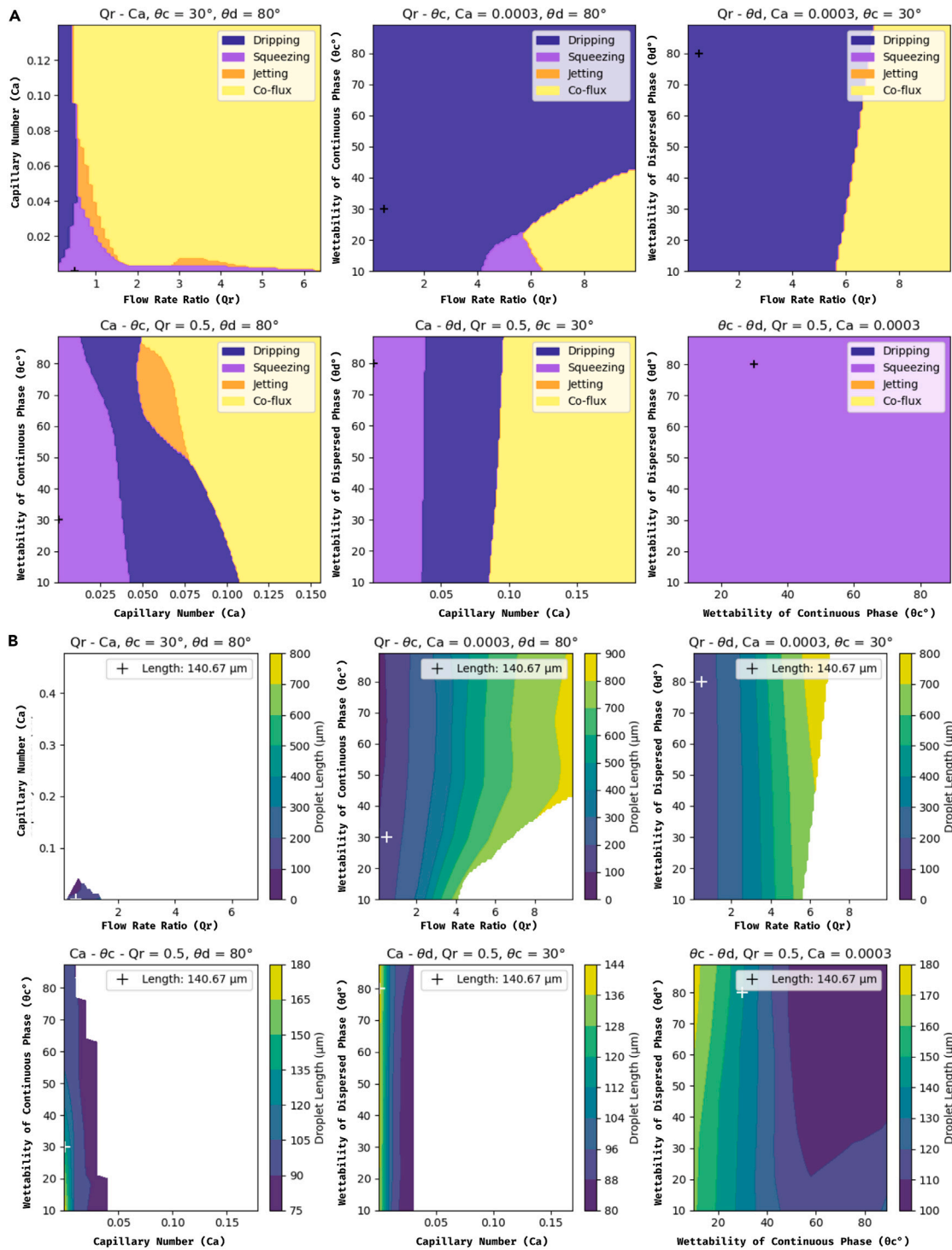


Figure 4. 2D maps' representation of the estimation of the droplet regime and length for a single set of input parameters

Six sets of 2D maps form the DL_r and the DL_r results for (A) regime and (B) droplet length estimation for input parameters of $Q_r = 0.5$, $Ca = 0.0003$, $\theta_c = 30^\circ$, and $\theta_d = 80^\circ$ selected from²⁶ and marked with '+' sign. See also Figures S8–S15.

STAR★METHODS

Detailed methods are provided in the online version of this paper and include the following:

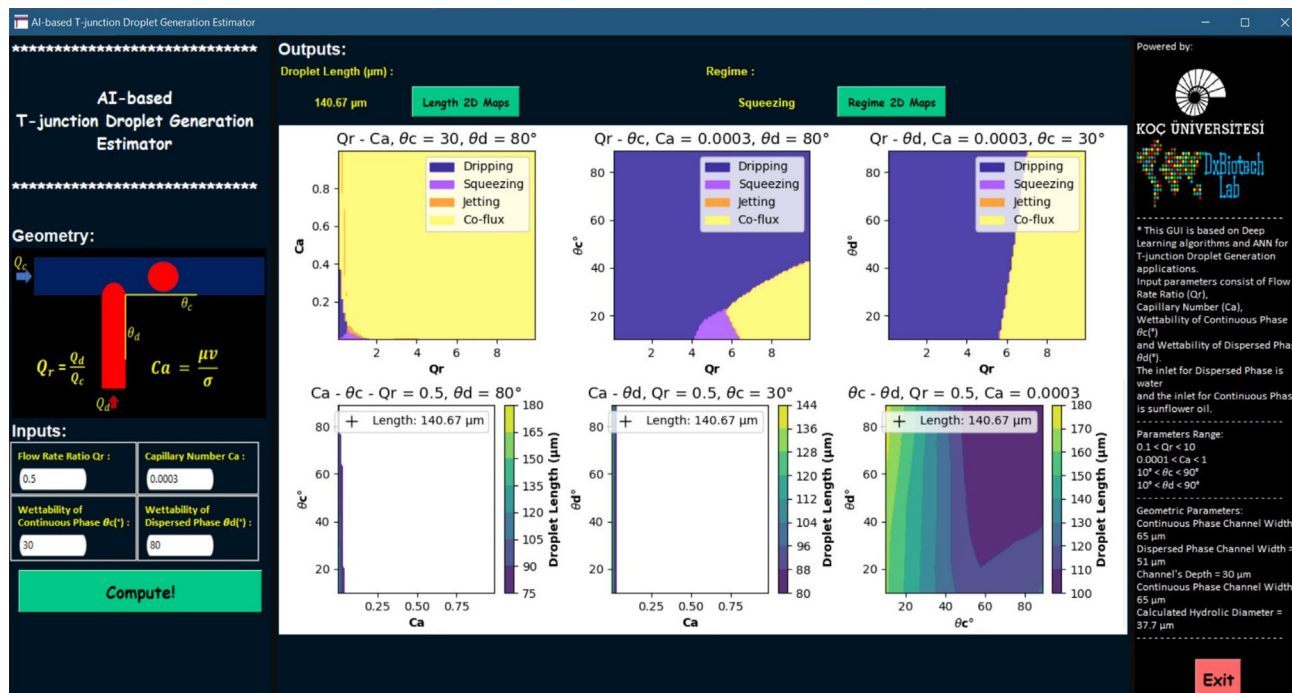


Figure 5. The graphical user interface (GUI) crafted for the estimation of droplet length and regime within the framework of the proposed T-junction droplet generation model

The DL_L module is utilized for the calculation of droplet length, and the DL_R module used is for determining the regime. 2D maps illustrating each combination of input parameters are shown in both modules.

- KEY RESOURCES TABLE
- RESOURCE AVAILABILITY
 - Lead contact
 - Materials availability
 - Data and code availability
- METHOD DETAILS

SUPPLEMENTAL INFORMATION

Supplemental information can be found online at <https://doi.org/10.1016/j.isci.2024.109326>.

ACKNOWLEDGMENTS

S.T. acknowledges Tubitak 2232 International Fellowship for Outstanding Researchers Award (118C391), Alexander von Humboldt Research Fellowship for Experienced Researchers, Marie Skłodowska-Curie Individual Fellowship (101003361), and Royal Academy NewtonKatip Çelbebi Transforming Systems Through Partnership Award (12N019) for financial support of this research. Opinions, interpretations, conclusions, and recommendations are those of the author and are not necessarily endorsed by the TÜBİTAK. This work was partially supported by Science Academy's Young Scientist Awards Program (BAGEP), Outstanding Young Scientists Awards (GEBİP), and Bilim Kahramanları Derneği The Young Scientist Award. This study was conducted using the service and infrastructure of Koç University Translational Medicine Research Center (KUTTAM). The authors have no other relevant affiliations or financial involvement with any organization or entity with a financial interest in or financial conflict with the subject matter or materials discussed in the manuscript apart from those disclosed.

AUTHOR CONTRIBUTIONS

Conceptualization, A.A., M.S., and S.T.; methodology, A.A., M.S., and S.T.; software, A.A.; validation, A.A. and M.S.; formal analysis, A.A. and M.S.; writing—original draft preparation, A.A.; writing—review and editing, M.S. and S.T.; supervision, S.T.; project administration, S.T.; funding acquisition, S.T. All authors have read and agreed to the published version of the manuscript.

DECLARATION OF INTERESTS

Authors declare no conflict of interest.

Received: December 19, 2023

Revised: January 13, 2024

Accepted: February 20, 2024

Published: February 28, 2024

REFERENCES

- Feng, H., Zheng, T., Li, M., Wu, J., Ji, H., Zhang, J., Zhao, W., and Guo, J. (2019). Droplet-based microfluidics systems in biomedical applications. *Electrophoresis* 40, 1580–1590.
- Weibel, D.B., and Whitesides, G.M. (2006). Applications of microfluidics in chemical biology. *Curr. Opin. Chem. Biol.* 10, 584–591.
- Ahmadpour, A., Isgor, P.K., Ural, B., Eren, B.N., Sarabi, M.R., Muradoglu, M., and Tasoglu, S. (2023). Microneedle arrays integrated with microfluidic systems: Emerging applications and fluid flow modeling. *Biomicrofluidics* 17, 021501.
- Ghaderinezhad, F., Ceylan Koydemir, H., Tseng, D., Karınca, D., Liang, K., Ozcan, A., and Tasoglu, S. (2020). Sensing of electrolytes in urine using a miniaturized paper-based device. *Sci. Rep.* 10, 13620.
- Dabbagh, S.R., Alseedi, M.M., Saadat, M., Sitti, M., and Tasoglu, S. (2022). Biomedical applications of magnetic levitation. *Adv. Nano Biomed. Res.* 2, 2100103.
- Sarabi, M.R., Ahmadpour, A., Yetisen, A.K., and Tasoglu, S. (2021). Finger-actuated microneedle array for sampling body fluids. *Appl. Sci.* 11, 5329.
- Yao, C., Liu, Y., Xu, C., Zhao, S., and Chen, G. (2018). Formation of liquid–liquid slug flow in a microfluidic T-junction: Effects of fluid properties and leakage flow. *AIChE J.* 64, 346–357.
- Guo, M.T., Rotem, A., Heyman, J.A., and Weitz, D.A. (2012). Droplet microfluidics for high-throughput biological assays. *Lab Chip* 12, 2146–2155.
- Adamo, A., Beingessner, R.L., Behnam, M., Chen, J., Jamison, T.F., Jensen, K.F., Monbaliu, J.-C.M., Myerson, A.S., Revalor, E.M., Snead, D.R., et al. (2016). On-demand continuous-flow production of pharmaceuticals in a compact, reconfigurable system. *Science* 352, 61–67.
- Zhou, F., Zhang, B., Yao, C., Zhu, K., Yang, M., and Chen, G. (2016). Cyclization of pseudoionone catalyzed by sulfuric acid in a microreactor. *Chem. Eng. Technol.* 39, 849–856.
- Elvira, K.S., Casadevall i Solvas, X., Wootton, R.C.R., and Demello, A.J. (2013). The past, present and potential for microfluidic reactor technology in chemical synthesis. *Nat. Chem.* 5, 905–915.
- Zhao, C.-X. (2013). Multiphase flow microfluidics for the production of single or multiple emulsions for drug delivery. *Adv. Drug Deliv. Rev.* 65, 1420–1446.
- Liu, D., Sun, M., Zhang, J., Hu, R., Fu, W., Xuanyuan, T., and Liu, W. (2022). Single-cell droplet microfluidics for biomedical applications. *Analyst* 147, 2294–2316.
- Skurtys, O., and Aguilera, J.M. (2008). Applications of microfluidic devices in food engineering. *Food Biophys.* 3, 1–15.
- Susanti, Winkelman, J.G.M., Schuur, B., Heeres, H.J., and Yue, J. (2016). Lactic acid extraction and mass transfer characteristics in slug flow capillary microreactors. *Ind. Eng. Chem. Res.* 55, 4691–4702.
- Yang, L., Zhao, Y., Su, Y., and Chen, G. (2013). An experimental study of copper extraction characteristics in a T-junction microchannel. *Chem. Eng. Technol.* 36, 985–992.
- Lefortier, S.G.R., Hamersma, P.J., Bardow, A., and Kreutzer, M.T. (2012). Rapid microfluidic screening of CO₂ solubility and diffusion in pure and mixed solvents. *Lab Chip* 12, 3387–3391.
- Foroughi, H., Abbasi, A., Das, K.S., and Kawaji, M. (2012). Immiscible displacement of oil by water in a microchannel: Asymmetric flow behavior and nonlinear stability analysis of core-annular flow. *Phys. Rev.* 85, 026309.
- Litster, S., Sinton, D., and Djilali, N. (2006). Ex situ visualization of liquid water transport in PEM fuel cell gas diffusion layers. *J. Power Sources* 154, 95–105.
- Wu, H., Odum, T.W., Chiu, D.T., and Whitesides, G.M. (2003). Fabrication of complex three-dimensional microchannel systems in PDMS. *J. Am. Chem. Soc.* 125, 554–559.
- Abdelgawad, M., Freire, S.L.S., Yang, H., and Wheeler, A.R. (2008). All-terrain droplet actuation. *Lab Chip* 8, 672–677.
- Zhu, P., and Wang, L. (2016). Passive and active droplet generation with microfluidics: a review. *Lab Chip* 17, 34–75.
- Li, X.-B., Li, F.-C., Yang, J.-C., Kinoshita, H., Oishi, M., and Oshima, M. (2012). Study on the mechanism of droplet formation in T-junction microchannel. *Chem. Eng. Sci.* 69, 340–351.
- Liu, H., and Zhang, Y. (2009). Droplet formation in a T-shaped microfluidic junction. *J. Appl. Phys.* 106, 034906.
- Liu, C., Zhu, C., Fu, T., Ma, Y., and Li, H.Z. (2019). Interfacial dynamics of the core-annular flow for glycerol–water solution/ionic liquid ([BMIM][PF₆]) two-phase flow in a microfluidic flow-focusing junction. *J. Taiwan Inst. Chem. Eng.* 98, 45–52.
- Venkateshwarlu, A., and Bharti, R.P. (2021). Effects of capillary number and flow rates on the hydrodynamics of droplet generation in two-phase cross-flow microfluidic systems. *J. Taiwan Inst. Chem. Eng.* 129, 64–79.
- Sontti, S.G., and Atta, A. (2017). CFD analysis of microfluidic droplet formation in non-Newtonian liquid. *Chem. Eng. J.* 330, 245–261.
- Thorsen, T., Roberts, R.W., Arnold, F.H., and Quake, S.R. (2001). Dynamic pattern formation in a vesicle-generating microfluidic device. *Phys. Rev. Lett.* 86, 4163–4166.
- Nisisako, T., Torii, T., and Higuchi, T. (2002). Droplet formation in a microchannel network. *Lab Chip* 2, 24–26.
- Xu, J.H., Li, S.W., Tan, J., Wang, Y.J., and Luo, G.S. (2006). Preparation of highly monodisperse droplet in a T-junction microfluidic device. *AIChE J.* 52, 3005–3010.
- Zeng, W., Tong, Z., Shan, X., Fu, H., and Yang, T. (2021). Monodisperse droplet formation for both low and high capillary numbers in a T-junction microdroplet generator. *Chem. Eng. Sci.* 243, 116799.
- Zeng, W., Yang, S., Liu, Y., Yang, T., Tong, Z., Shan, X., and Fu, H. (2022). Precise monodisperse droplet generation by pressure-driven microfluidic flows. *Chem. Eng. Sci.* 248, 117206.
- Loizou, K., Wong, V.-L., Thielemans, W., and Hewakandamby, B. (2014). Effect of Fluid Properties on Droplet Generation in a Microfluidic T-Junction (Fluids Engineering Division Summer Meeting).
- Loizou, K., Wong, V.-L., and Hewakandamby, B. (2018). Examining the effect of flow rate ratio on droplet generation and regime transition in a microfluidic T-junction at constant capillary numbers. *Inventions* 3, 54.
- Wehking, J.D., Gabany, M., Chew, L., and Kumar, R. (2014). Effects of viscosity, interfacial tension, and flow geometry on droplet formation in a microfluidic T-junction. *Microfluid. Nanofluidics* 16, 441–453.
- Chen, Y., and Deng, Z. (2017). Hydrodynamics of a droplet passing through a microfluidic T-junction. *J. Fluid Mech.* 819, 401–434.
- Glawdel, T., and Ren, C.L. (2012). Droplet formation in microfluidic T-junction generators operating in the transitional regime. III. Dynamic surfactant effects. *Phys. Rev.* 86, 026308.
- Zhang, J., Zhang, X., Zhao, W., Liu, H., and Jiang, Y. (2022). Effect of surfactants on droplet generation in a microfluidic T-junction: A lattice Boltzmann study. *Phys. Fluids*, 34.
- Liu, J., and Trung Nguyen, N. (2010). Numerical simulation of droplet-based microfluidics-A review. *Micro Nanosyst.* 2, 193–201.
- Zhang, J. (2011). Lattice Boltzmann method for microfluidics: models and applications. *Microfluid. Nanofluid.* 10, 1–28.
- Liu, H., and Zhang, Y. (2011). Lattice Boltzmann simulation of droplet generation in a microfluidic cross-junction. *Commun. Comput. Phys.* 9, 1235–1256.
- Chekifi, T. (2018). Computational study of droplet breakup in a trapped channel configuration using volume of fluid method. *Flow Meas. Instrum.* 59, 118–125.
- Han, W., Chen, X., Hu, Z., and Yang, K. (2018). Three-dimensional numerical simulation of a droplet generation in a double T-junction microchannel. *J. Micro/Nanolith. MEMS MOEMS* 17, 1–025502.
- Nuhn, J.A.M., Gong, S., Che, X., Que, L., and Schneider, I.C. (2018). Microtissue size and cell-cell communication modulate cell migration in arrayed 3D collagen gels. *Biomed. Microdevices* 20, 62–69.
- Che, X., Nuhn, J., Schneider, I., and Que, L. (2016). High throughput studies of cell migration in 3D microtissues fabricated by a droplet microfluidic chip. *Micromachines* 7, 84.
- Temirel, M., Yenilmez, B., and Tasoglu, S. (2021). Long-term cyclic use of a sample collector for toilet-based urine analysis. *Sci. Rep.* 11, 2170.
- Lashkaripour, A., Rodriguez, C., Mehdipour, N., Mardian, R., McIntyre, D., Ortiz, L.,

- Campbell, J., and Densmore, D. (2021). Machine learning enables design automation of microfluidic flow-focusing droplet generation. *Nat. Commun.* 12, 25.
48. Srikanth, S., Dubey, S.K., Javed, A., and Goel, S. (2021). Droplet based microfluidics integrated with machine learning. *Sensor Actuator Phys.* 332, 113096.
 49. Zhang, S., Liang, X., Huang, X., Wang, K., and Qiu, T. (2022). Precise and fast microdroplet size distribution measurement using deep learning. *Chem. Eng. Sci.* 247, 116926.
 50. Dabbagh, S.R., Rabbi, F., Doğan, Z., Yetisen, A.K., and Tasoglu, S. (2020). Machine learning-enabled multiplexed microfluidic sensors. *Biomicrofluidics* 14, 061506.
 51. Rezapour Sarabi, M., Alseed, M.M., Karagoz, A.A., and Tasoglu, S. (2022). Machine learning-enabled prediction of 3D-printed microneedle features. *Biosensors* 12, 491.
 52. Das, S., Dey, A., Pal, A., and Roy, N. (2015). Applications of artificial intelligence in machine learning: review and prospect. *Int. J. Comput. Appl.* 115, 31–41.
 53. Dunjko, V., and Briegel, H.J. (2018). Machine learning & artificial intelligence in the quantum domain: a review of recent progress. *Rep. Prog. Phys.* 81, 074001.
 54. Stafford, I.S., Kellermann, M., Mossotto, E., Beattie, R.M., MacArthur, B.D., and Ennis, S. (2020). A systematic review of the applications of artificial intelligence and machine learning in autoimmune diseases. *NPJ Digit. Med.* 3, 30.
 55. Tasoglu, S. (2022). Toilet-based continuous health monitoring using urine. *Nat. Rev. Urol.* 19, 219–230.
 56. Balbach, S., Jiang, N., Moreddu, R., Dong, X., Kurz, W., Wang, C., Dong, J., Yin, Y., Butt, H., Brischwein, M., et al. (2021). Smartphone-based colorimetric detection system for portable health tracking. *Anal. Methods* 13, 4361–4369.
 57. Yu, Z., Jiang, N., Kazarian, S.G., Tasoglu, S., and Yetisen, A.K. (2021). Optical sensors for continuous glucose monitoring. *Prog. Biomed. Eng.* 3, 022004.
 58. Talebjedi, B., Abouei Mehrizi, A., Talebjedi, B., Mohseni, S.S., Tasnim, N., and Hoorfar, M. (2022). Machine learning-aided microdroplets breakup characteristic prediction in flow-focusing microdevices by incorporating variations of cross-flow tilt angles. *Langmuir* 38, 10465–10477.
 59. Chagot, L., Quilodrán-Casas, C., Kalli, M., Kovalchuk, N.M., Simmons, M.J.H., Matar, O.K., Arcucci, R., and Angeli, P. (2022). Surfactant-laden droplet size prediction in a flow-focusing microchannel: a data-driven approach. *Lab Chip* 22, 3848–3859.
 60. Shojaeian, M., and Hardt, S. (2018). Fast electric control of the droplet size in a microfluidic T-junction droplet generator. *Appl. Phys. Lett.* 112, 194102.
 61. Xu, M., Watanachaturaporn, P., Varshney, P., and Arora, M. (2005). Decision tree regression for soft classification of remote sensing data. *Remote Sens. Environ.* 97, 322–336.
 62. Ahmadvpour, A., Yetisen, A.K., and Tasoglu, S. (2023). Piezoelectric Metamaterial Blood Pressure Sensor. *ACS Appl. Electron. Mater.*
 63. Zupan, J. (1994). Introduction to artificial neural network (ANN) methods: what they are and how to use them. *Acta Chim. Slov.* 41, 327.

STAR★METHODS

KEY RESOURCES TABLE

REAGENT or RESOURCE	SOURCE	IDENTIFIER
Software and algorithms		
COMSOL Multiphysics	COMSOL, Inc. 100 District Avenue Burlington, MA 01803, USA	N/A
MATLAB Software	MathWorks, 3 Apple Hill Drive, Natick, MA 01760, USA	N/A
scikit-learn	Python library	N/A
TensorFlow	Python framework	N/A
Tkinter	Python toolkit	N/A

RESOURCE AVAILABILITY

Lead contact

Further information and requests for resources and reagents should be directed to and will be fulfilled by the lead contact, Savas Tasoglu (stasoglu@ku.edu.tr).

Materials availability

This study did not use any new materials.

Data and code availability

- All data reported in this paper will be shared by the [lead contact](#) upon request.
- This paper does not report the original code.
- Any additional information required to reanalyze the data reported in this paper is available from the [lead contact](#) upon request.

METHOD DETAILS

T-junction droplet simulations were employed using COMSOL Multiphysics software, where initial settings governed oil-water interaction. Utilizing Livelink MATLAB, phase-defined droplet images were generated and stored for various parameters. Subsequent FEA generated images underwent binary image analysis to enhance parameter measurement during droplet formation. Key parameters extracted from binary images were Regime and Droplet Length, crucial for the research objectives. Each image scenario yielded two numerical outputs, resulting in a dataset comprising 8020 data points. Machine ML and DL techniques were then employed using scikit-learn library and TensorFlow framework in Python to train models for droplet regime classification and droplet length regression. These trained models were applied to estimate key outputs for the T-junction droplet generation setup. The GUI was developed using Tkinter toolkit in Python to estimate droplet length and regime within the proposed T-junction droplet generation model.